Interrelationship among dielectric constant, energy band parameters and ionicity in multi-component oxide glasses revealed by optical- and THz-band spectroscopy

Wada, Osamu
Ramachari, Doddoji
Yang, Chan-Shan
Pan, Ci-Ling

(Citation)
Journal of Non-Crystalline Solids,573:121135

(Issue Date)
2021-12-01

(Resource Type)
journal article

(Version)
Version of Record

(URL)
https://hdl.handle.net/20.500.14094/90008713

Journal of Non-Crystalline Solids 573 (2021) 121135

Contents lists available at ScienceDirect

Journal of Non-Crystalline Solids

journal homepage: www.elsevier.com/locate/jnoncrysol

Interrelationship among dielectric constant, energy band parameters and ionicity in multi-component oxide glasses revealed by optical- and THz-band spectroscopy

Osamu Wada [a,b,*], Doddoji Ramachari [c,d], Chan-Shan Yang [e,f], Ci-Ling Pan [a]

[a] Department of Physics, National Tsing Hua University, Hsinchu 30013, Taiwan
[b] Office for Academic and Industrial Innovation, Kobe University, Kobe 657-8501, Japan
[c] Institute of Research and Development, Duy Tan University, Da Nang 550000, Vietnam
[d] Faculty of Natural Sciences, Duy Tan University, Da Nang 550000, Vietnam
[e] Institute and Undergraduate Program of Electro-Optical Engineering, National Taiwan Normal University, Taipei 11677, Taiwan
[f] Micro/Nano Device Inspection and Research Center, National Taiwan Normal University, Taipei 106, Taiwan

ARTICLE INFO

Keywords:
Dielectric constant
Bandgap energy
Ionicity
Multi-component silicate oxide glasses
Optical spectroscopy
THz spectroscopy

ABSTRACT

The dielectric constant, energy band parameters and ionicity are key physical parameters for fully understanding the dielectric properties of glasses, but their mutual interrelationship and its applicability to a wide variety of multi-component glasses have not yet been confirmed. We have applied the optical and THz spectroscopic characterization to a set of multi-component silicate oxide glasses incorporating vastly different additive components. The key physical parameters evaluated in the optical region have been interpreted consistently by the single oscillator based dielectric model. The bandgap energy (E_g) and ionicity parameter (Wemple and DiDomenico's β parameter) estimated in the optical region have shown reasonable correspondence, respectively, with the homopolar energy (E_h) and the polarization ionicity (I_P) which are evaluated from the THz dielectric constant measurement. The comprehensive interrelation thus confirmed has provided simple rules between the physical parameters without limitation of glass compositions. For example, a tradeoff relation between the oscillator strength and characteristic resonance wavelength and a simple correlation between the dielectric constant and bandgap energy have been determined for the present set of multi-component glasses. The energy band parameters have been used for deriving the joint density of state diagrams, and characteristic physical/chemical nature has been identified to each glass.

Introduction

High refractive index glass materials are prerequisite for optical components such as lenses, fibers, waveguides and various active devices which are essential for developing systems in optical, infrared and terahertz (THz) frequency ranges. Currently demanded topics of glass research include the development of high dielectric constant glasses useful in the THz frequency range (0.1–10 THz) [1-4]. Recent studies on THz dielectric properties of a variety of glasses using THz time domain spectroscopy (THz-TDS) measurements have shown that some of the existing multi-component glasses, for example silicate oxide glasses [5] and chalcogenide glasses [6], possess high dielectric constant values useful in THz range. We have recently reported that oxyfluorosilicate (OFS) glasses exhibit very low loss (down to 6–9 cm^{-1}) and high dielectric constant (2.9–3.7) at 0.5 THz [7,8], which indicates their usefulness in short distance waveguides and compact devices in the sub-THz frequency range.

There is no doubt about the critical importance of understanding the physical reason and mechanism of such enhancement in the dielectric constant. In our recent work [8], we have conducted detailed analysis of the dielectric properties as determined from the THz-TDS data by using the Lorentz model. This work has demonstrated that the dielectric properties of a wide variety of multi-component silicate oxide glasses are consistently interpreted by a unified single oscillator model [8]. The dielectric constant in the THz region directly reflects the ionic vibration, therefore the ionic/covalent nature of chemical bonding of the material is readily observed by the THz measurements. Taking an example of a multi-component silicate oxide glass, when modifier or intermediate

* Corresponding author.
E-mail address: fwga3962@nifty.com (O. Wada).

https://doi.org/10.1016/j.jnoncrysol.2021.121135
Received 22 May 2021; Received in revised form 11 August 2021; Accepted 19 August 2021
Available online 30 August 2021

network former atoms are added to SiO_2, the basic three dimensional network structure based on SiO_4 tetrahedral arrays is reorganized or modified, through the replacement of cations (Si) or physical/chemical modification of Si-O links, and result in the resonant frequency shifts and oscillator strength variations for the oscillators of ionic vibration. In our most recent study [9], in which the local field correction and polarization ionicity effect are incorporated into the single Lorentz oscillator model, significant influence of ionicity has been revealed in the dielectric constant variation inbetween the THz and optical frequencies for the same wide variety of the multi-component silicate oxide glasses as tested in [8]. Such analyses have enabled novel findings in glasses' structural/chemical nature such as an increase of the effective ionic charge of oscillator in high-THz dielectric constant OFS glasses [9]. Those recent works have demonstrated the unique advantage of using THz characterization to focus the impact of the ionic contribution to the dielectric property, which is often hidden behind when only usual optical characteristics are investigated.

The bandgap energy in oxide glasses is defined as the electron transition energy for valence electrons of oxygen ions to the excited states (conduction band). Because of the long range periodicity and symmetry lost in glass structures, the band edge shape exhibits broadening as compared with that in crystals, but the bandgap energy still reflects the short range ordering and provides useful information on valence electrons and band structure in the material. Since most of the glasses used in infrared and THz applications have bandgap energies in the optical frequency region, there have been numerous studies to attempt to correlate the dielectric constant (refractive index), bandgap energy and other parameters in optical frequency range for various glasses [10-13]. The ionicity/covalency of materials is another important parameter to investigate the interrelation between the dielectric properties and atomic bonds in the material, as seen in the THz range [8,9] as mentioned above. Wemple and DiDomenico (WDD) [14] have analyzed the optical dielectric constant dispersion properties by applying basically the single Lorentz oscillator model, in which they have introduced a unique constant to distinguish the ionicity (ionic or covalent bond) in a variety of materials. In Phillips and Van Vechten's (PVV) theory [15] based on the Penn gap model [16] of the optical dielectric constant, contributions of the homopolar/heteropolar energies have been analyzed to determine the ionicity of material. Although those characterization schemes have shown reasonable successes in crystalline and amorphous solids having rather simple compositions [10-15], their applicability to multi-component glasses with complicated compositions have not been studied satisfactorily so far. As for the ionicity evaluation, there have been no investigations on the relationship between the ionicity parameters as determined by optical dispersion as mentioned above [14,15] and that (polarization ionicity) as determined by the THz measurements as reported previously by us [9]. Thus the issue of existing characterization methods we should clarify is twofold: one is the correlations among different physical parameters, and the other is the applicability of such correlations to vastly different glass compositions.

The main objective of the present work is to determine the dielectric constant, energy band parameter, and ionicity properties in the optical frequency region and clarify their interrelationship with the properties determined in the THz frequency region over a wide variety of multi-component silicate oxide glasses. This study provides the comprehensive determination of a set of physical parameters to each glass, and verifies the correspondence of the ionicity parameters determined in both the optical and THz regions. Also the determined energy band parameters can be used to derive the joint density of state diagram for each glass so that one can discuss physical and chemical nature of a specific glass.

In the following, after mentioning the experimental technique we analyze and discuss the dielectric constant and bandgap energy properties in the optical region by using WDD model. We then look into the ionicity effect by using the measured results of THz dielectric constant and by applying WDD model as well as PVV model. We finally illustrate and discuss the joint density of state diagrams of representative glasses.

2. Experimental technique

The multi-component silicate oxide glasses adopted in this study include our own OFS glasses and several other commercial glasses. Compositions and basic physical parameters of glasses, the molecular weight M, specific density ρ, and molar volume $V_m=M/\rho$, are summarized in Table 1 [7]. OFS glasses were prepared by the melt-quenching technique as reported in our earlier paper [7,8]. The optical transmission and reflectivity were measured by using the conventional Fourier transform infrared (FTIR) spectroscopy system in the visible to near-infrared range, and the dispersion properties of optical refractive indices and absorption coefficients were determined using the standard methods [8]. The THz dielectric constant properties of OFS glasses were measured by using a photoconductive-antenna-based transmission type THz-TDS system [17] and the results have been already reported in [7,8]. As for commercial glasses used in this study, the optical dielectric constant and absorption characteristics data were taken from data sheets [18,19; for silica: 20] and the THz dielectric properties were taken from Naftaly's publication [5]. Considering the measurement accuracy and calculation precision, the significant figures of all the data values used or quoted in all equations, tables and figures in this paper have been set as three digits.

3. Results and discussion

3.1. Optical dielectric constant

The dielectric constant dispersion characteristics in the frequency region below the bandgap can be analyzed by using the WDD single oscillator model [14]. The optical dielectric constant ε(hν) at the photon energy of hν (h is Planck's constant and ν is the frequency) is basically expressed by $\varepsilon(h\nu) = n_{opt} + ik$, where n_{opt} is the optical refractive index and k is the extinction coefficient. However, in all of present glasses k is orders of magnitude smaller than n_{opt} (for example, $k < 2 \times 10^{-5}$ and $n_{opt} > 1.5$ for the present OFS glasses in the range of $h\nu = 0.6$–3.2 eV), the optical refractive index is a real value and is approximated by $\varepsilon(h\nu)= {n_{opt}}^2$. In WDD model, the optical dielectric constant is expressed by:

$$\varepsilon(h\nu) - 1 = \frac{E_d E_0}{{E_0}^2 - (h\nu)^2}, \tag{1}$$

where E_0 and E_d are the oscillator energy and dispersion energy, respectively. E_0 represents the average bandgap which corresponds to the difference between the center of gravity energies of the valence and conduction bands. E_d represents the average strength of interband optical transitions [21]. This equation can be converted into the following form using the wavelength λ:

$$\frac{1}{\varepsilon(h\nu) - 1} = \frac{{\lambda_0}^2}{\varepsilon_\infty - 1}\left(\frac{1}{{\lambda_0}^2} - \frac{1}{\lambda^2}\right), \tag{2}$$

where λ_0 is the oscillator characteristic wavelength and we use ε_∞ to denote the optical dielectric constant at a frequency much lower than the characteristic frequency ($\lambda \to \infty$ in Eq. (2)) following the convention. Eq. (2) indicates that the plot of $1/(\varepsilon(h\nu)-1)$ versus λ^{-2} results in a straight line, and that ε_∞ is given by $\varepsilon_\infty = 1 + 1/(\text{y-intercept})$ and λ_0 is given by $\lambda_0 = (\text{slope})/(\text{y-intercept})$. Then the value of E_0 is determined by $E_0 = hc/\lambda_0$ and E_d by $E_d = hc(\varepsilon_\infty - 1)/\lambda_0$, respectively, where c is the light velocity. Fig. 1 shows the result of such plots for (a) ZNbKLSNd glasses, (b) PbNKLSNd glasses, and (c) other multi-component silicate oxide glasses. As shown in the figures, plots obey straight lines and E_0 and E_d are readily determined. Although an oscillatory behavior by unknown reason was seen in one of the plot (PbNKLSNd05), linear approximation was adopted, since this sample showed normal behaviors in other

Table 1
Compositions and basic physical parameters of a variety of silicate oxide glasses.

Glass	Composition		M (g/mol)	ρ (g/cm^3)	V_m (cm^3/mol)	Ref
ZNbKLSNdx	(20-x)ZnF_2+20Nb_2O_5+20K_2CO_3+ 10LiF+30SiO_2 +xNd_2O_3	$x = 1$	124	3.65	34.0	[7,8]
		$x = 5$	133	3.66	36.3	
		$x = 10$	145	3.54	41.0	
PbNKLSNdx	(20-x)PbF_2+5Na_2O+20K_2CO_3+ 10LiF+45SiO_2+ xNd_2O_3	$x = 1$	110	3.72	29.7	[7,8]
		$x = 5$	114	3.78	30.2	
		$x = 10$	119	3.62	32.8	
Silica	SiO_2		60	2.20	27.3	[7,8]
Pyrex	80.6SiO_2+12.6B_2O_3+4.2Na_2O+2.2Al_2O_3+0.04Fe_2O_3+0.1CaO+0.05MgO+0.1Cl		62	2.23	27.8	[7,8]
BK7	68.9SiO_2+10.1B_2O_3+8.8Na_2O+8.4K_2O+2.8BaO+1.0As_2O_3		65	2.51	26	[7,8]
SK10	30.6SiO_2+11.7B_2O_3+5.0Al_2O_3+0.1Na_2O+48.2BaO+2.0ZnO+0.7PbO+0.8Sb_2O_3+0.9As_2O_3		112	3.64	30.8	[7,8]
SF10	35.3SiO_2+2.0Na_2O+2.5K_2O+55.7PbO+4.0TiO_2+0.5As_2O_3		153	4.28	35.8	[7,8]
SF6	27.7SiO_2+0.5Na_2O+1.0K_2O+70.5PbO+0.3As_2O_3		177	5.18	34.2	[7,8]

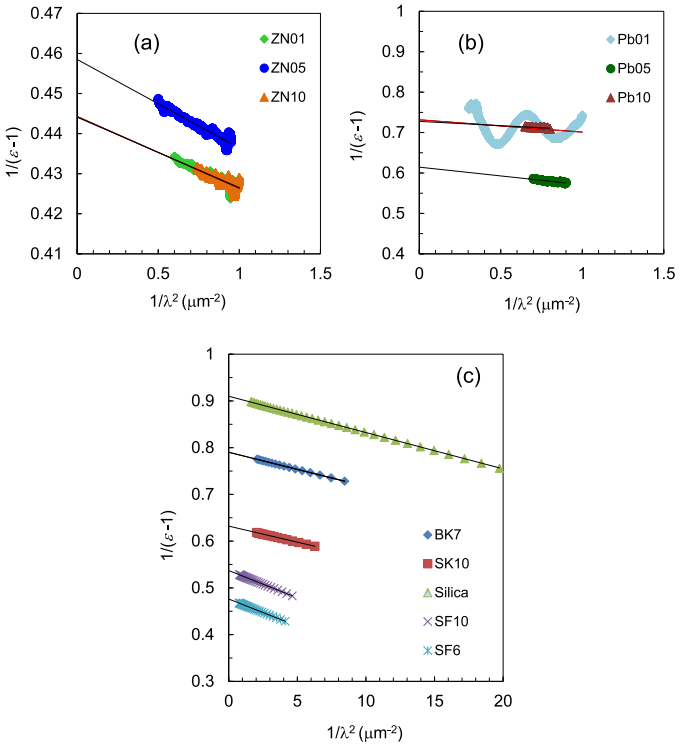

Fig. 1. Relationships of $1/(\varepsilon(h\nu)-1)$ as functions of λ^{-2} for (a) ZNbKLSNd glasses, (b) PbNKLSNd glasses, and (c) other multi-component silicate oxide glasses.

measurements. The resulted values of E_0 and E_d are included in Table 2. Fig. 2 shows a plot of the optical dielectric constant measured at the wavelength of 1550 nm, ε_{opt}, as a function of E_d/E_0. This shows an excellent fit with the straight line $\varepsilon_\infty = 1 + E_d/E_0$ which is deduced from Eq.(1) for zero frequency, confirming the applicability of this oscillator model for all the multi-component glasses.

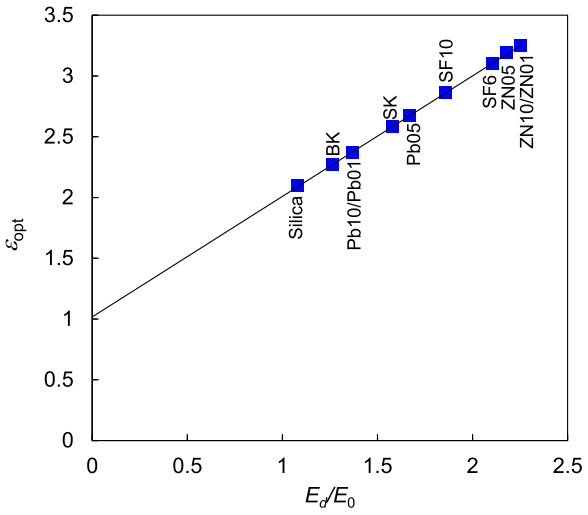

Fig. 2. Relationship between the optical dielectric constant measured at the wavelength of 1550 nm, ε_{opt}, as a function of E_d/E_0. The fitted straight line indicates the agreement of experimental data with Eq. (1) at low frequency limit.

Eq. (1) is essentially equivalent with the dielectric function based on Lorentz model with the damping term neglected in the frequency region well below the transition (also called Drude-Voigt equation [22]), as shown by:

$$\varepsilon(\hbar\omega) - 1 = \frac{Ne^2}{\varepsilon_0 m}\frac{f}{{\omega_0}^2 - \omega^2}, \tag{3}$$

Table 2
The physical parameters determined from optical measurements for a variety of glasses, including the optical dielectric constant (ε_∞), characteristic resonance wavelength (λ_0), dispersion energy (E_d), oscillator energy (E_0), bandgap energy (E_g), Urbach energy (E_U), oscillator strength (f) and its proportionality factor ($E_dE_0V_m$).

Glass	ε_∞	λ_0(μm)	E_d (eV)	E_0 (eV)	E_d/E_0	E_g (eV)	E_U (eV)	E_0/E_g (*Av.* k" =2.30)	$E_dE_0V_m$(x10^3 eV^{2}cm^3/mol)	f
ZNbKLSNd01	3.25	0.201	13.9	6.17	2.25	3.21	0.203	1.92	2.91	0.0889
ZNbKLSNd05	3.19	0.220	12.3	5.65	2.18	3.19	0.212	1.77	2.53	0.0771
ZNbKLSNd10	3.25	0.200	14.0	6.21	2.25	3.18	0.205	1.95	3.56	0.109
PbNKLSNd01	2.37	0.204	8.30	6.07	1.37	3.55	0.123	1.71	1.49	0.0456
PbNKLSNd05	2.67	0.201	10.3	6.17	1.67	3.48	0.128	1.77	1.92	0.0584
PbNKLSNd10	2.37	0.170	10.0	7.30	1.37	3.44	0.142	2.12	2.39	0.0729
silica	2.10	0.0924	14.5	13.4	1.08	7.20	0.107	1.86	5.30	0.162
Pyrex	2.16					3.85				
BK7	2.27	0.0963	16.3	12.9	1.26	3.80	0.161	3.39	5.47	0.167
SK10	2.58	0.104	18.8	11.9	1.58	3.42	0.144	3.48	6.88	0.210
SF10	2.86	0.148	15.6	8.40	1.86	3.15	0.106	2.67	4.68	0.143
SF6	3.10	0.155	16.8	7.98	2.11	3.06	0.113	2.61	4.58	0.140

where $\hbar = h/2\pi$, h is the Planck's constant, ω is the angular frequency, N is the number of oscillator in a unit volume ($N = N_A/V_m$, N_A: Avogadro number), ε_0 is the dielectric constant of vacuum, e is the electronic unit charge, m is the electron mass, f is the oscillator strength for the transition at the energy of $\hbar\omega_0$, and ω_0 is the characteristic angular frequency correlated with λ_0 by $\omega_0 = 2\pi c/\lambda_0$. A comparison of Eqs. (1) to Eq. (3) leads to an expression which determines the oscillator strength f:

$$f = \frac{\varepsilon_0 m}{N_A \hbar^2} E_d E_0 V_m = 3.05 \times 10^{-5} E_d E_0 V_m, \quad (4)$$

where $E_0$and E_d are in eV and V_m is in cm^3/mol. Also λ_0 is written by using E_0 as $\lambda_0 = 2\pi c/\omega_0 = hc/E_0$. The oscillator strength values calculated from Eq. (4) are included in Table 2. Fig. 3 shows a relationship of the specimen specific proportionality factor $E_dE_oV_m$ of the oscillator strength f as a function of the characteristic wavelength $\lambda_0$for all the glasses examined. It is noticed that there is obviously a common trend of the decrease of $E_dE_oV_m$ for increasing λ_0 for all multi-component glasses regardless of the difference in additive components. A straight line obtained by the linear fit ($E_dE_0V_m$ (eV^2cm^3/mol) $= -3.17 \times 10^4 \lambda_0$ (μm) + 8.95×10^3) is shown in the figure for a guide for eye. Such a clear relation has not been reported in our knowledge for silicate oxide glasses, but similar trends have been observed on other glasses, for example, borate [23], tellurite, antimonite and heavy-metal oxide glasses [24]. In borate glasses ($BaO\text{-}M_mO_n\text{-}B_2O_3$ glass, M: cation) [23], small f and large λ_0 have been observed for high cation field strength (Z/a^2, Z: cation valence, a: cation-anion distance). The trend observed in Fig. 3 is considered to reflect the strength of chemical bond in the glass. Glasses with large f and small λ_0 such as silica, BK7 and SK10 glasses imply to have tighter bonds than ZNbKLSNd and PbNKLSNd glasses which exhibit, conversely, small f and large λ_0. It is observed in Table 1 and Table 2 that silica and BK7 glasses have small V_m and high bandgap energy (shown later), and conversely, ZNbKLSNd and PbNKLSNd glasses rather large V_m and low bandgap energy (shown later). This is consistent with the tighter bonding in the former glasses than in the latter.

3.2. Bandgap energy

The optical absorption coefficient (α) can be determined from the transmission spectrum as $\ln((1\text{-}R)^2/T)/d$, where R is the reflectance, T is the fractional transmission, d is the sample thickness and $(1\text{-}R)^2$ is a factor representing the Fresnel loss. $(1\text{-}R)^2$ is nearly constant in visible-infrared range for each sample (0.85–0.91 for OFS glasses). Considering that the object of the present analysis is to determine the energy dependence rather than the absolute value of α, we have used a simplified relation $\alpha = \ln(1/T)/d$ by neglecting the Fresnel loss. The optical absorption edge shape can be analyzed by using Tauc relation [25] and we apply the following formula to determine the optical bandgap energy relevant for allowed indirect transitions in amorphous materials:

$$\alpha h\nu = A(h\nu - E_g)^2, \quad (5)$$

where A is a constant specific to the transition in question. Fig. 4 shows the relationships of $(\alpha h\nu)^{1/2}$ as functions of hν for (a) ZNbKLSNd, (b) PbNKLSNd and (c) other multi-component glasses. The bandgap energy is determined from the energy intercept of the straight line fitting with the plots, and the results are shown in Table 2.

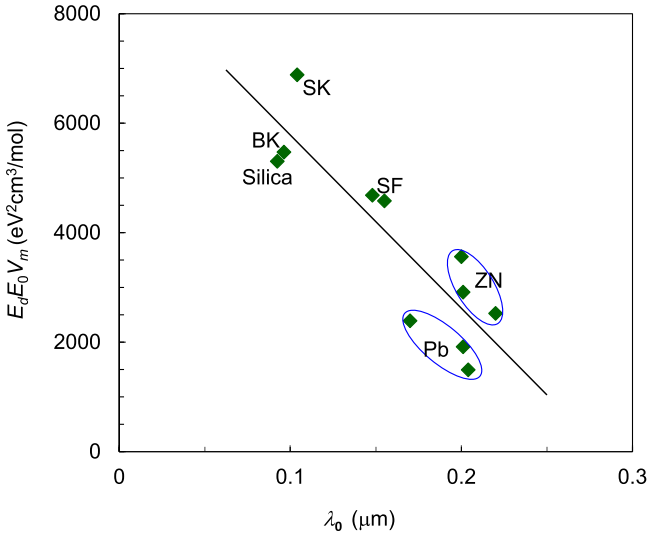

Fig. 3. Plots of the values of $E_dE_oV_m$ which represents the specimen specific proportionality factor for the oscillator strength f as a function of the characteristic wavelength $\lambda_0$for all the glasses examined. This indicates a tradeoff relation between f and λ_0, and the result of linear fit is indicated by a straight line.

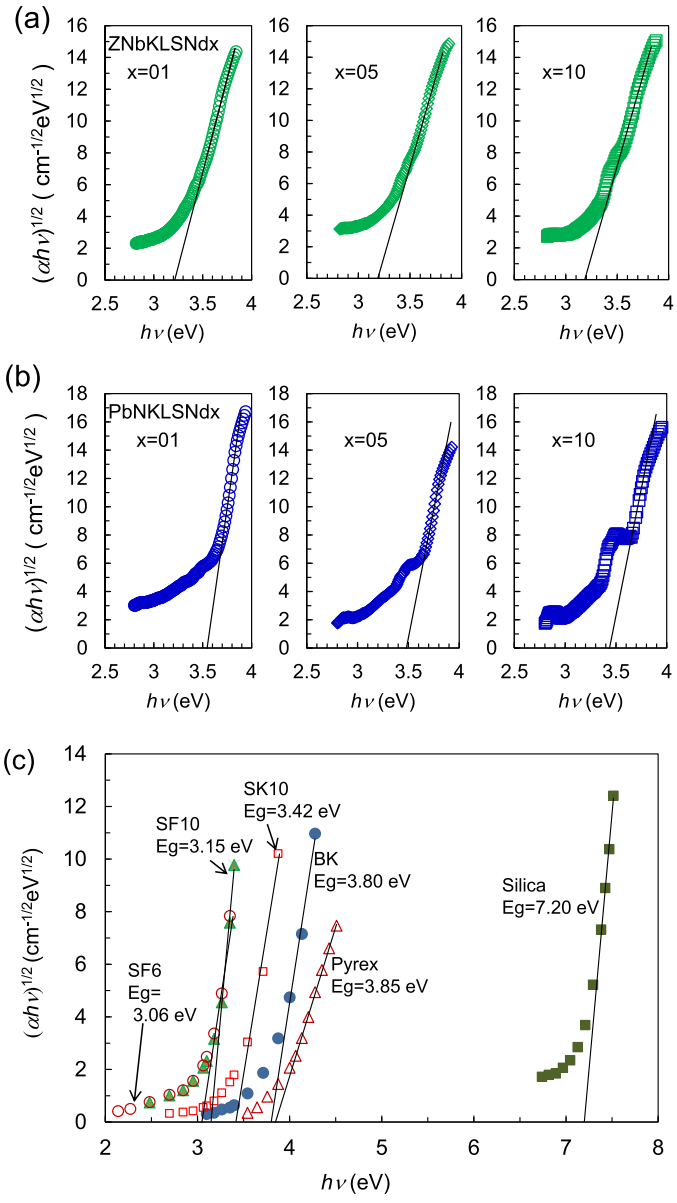

Fig. 4. Relationships of $(\alpha h\nu)^{1/2}$ as functions of hν for (a) ZNbKLSNd, (b) PbNKLSNd and (c) other multi-component glasses. The hν-axis intercept of the linear extrapolation of data gives the optical bandgap energy E_g.

An absorption tail can appear in the lower energy side of the main transition energy when localized state exists in the energy gap. This is called Urbach tail and is expressed by an exponential function [26]:

$$\alpha(h\nu) = \alpha_0 \exp(h\nu / E_U), \quad (6)$$

where α_0 is a constant and E_U is the Urbach energy. Fig. 5 shows lnα versus hν plots for (a) ZNbKLSNd and PbNKLSNd glasses and (b) other multi-component glasses. The Urbach energies calculated from the linear parts of the plots are shown in Table 2.

In Fig. 6 the determined values of E_g and E_U are plotted as functions of the optical dielectric constant ε_∞. E_g shows a high value for silica and sharply decreases as soon as additive elements begin to be incorporated in the glass, and thereafter E_g shows a monotonous variation with ε_∞. The sharp decrease of E_g due to the addition of very small amount of additives has been found also in other glasses [27-29], which implies a strong influence of the additive to the band structures. The large E_g decrease observed in multi-component glasses should be due to the small bandgap energies of constituent oxides such as Nb_2O_5 ($E_g = 3.4$ eV [11]), Na_2O (2.5 eV [10]), BaO (2.7 eV [10]), ZnO (3.4 eV [11]), and PbO (2.8 eV [11]). The monotonous relationship between E_g and ε_∞ or the optical refractive index n_{opt} ($n_{opt} = \varepsilon_\infty^{1/2}$) as found in all multi-component glasses (except silica) have been observed in many different solid materials, and a variety of approximation methods have been proposed [30,31]. A linear approximation [20] has been examined here for n_{opt}, and a relationship of $n_{opt} = -0.448\ E_g\ (eV) + 3.1669$ has been obtained as is shown in the inset of Fig. 6(a). On the other hand, as shown in Fig. 6(b), E_U is almost independent of ε_∞, and is considered to be controlled by the compositional/structural fluctuations and defects in each glass. Silica has the minimum value of E_U (0.109 eV) and as the additives are incorporated in the glass E_U seems to increase, and ZNbKLSNd glasses show the maximum value of E_U (0.212 eV). The Urbach tail is often ascribed by the tail states associated with either the conduction band or valence band. In Fig. 5(a) PbNKLSNd glasses exhibit characteristic shoulders in the energy dependence of absorption. We will come back to the discussion on the origins of those absorption tails and shoulders in Section 3.5.

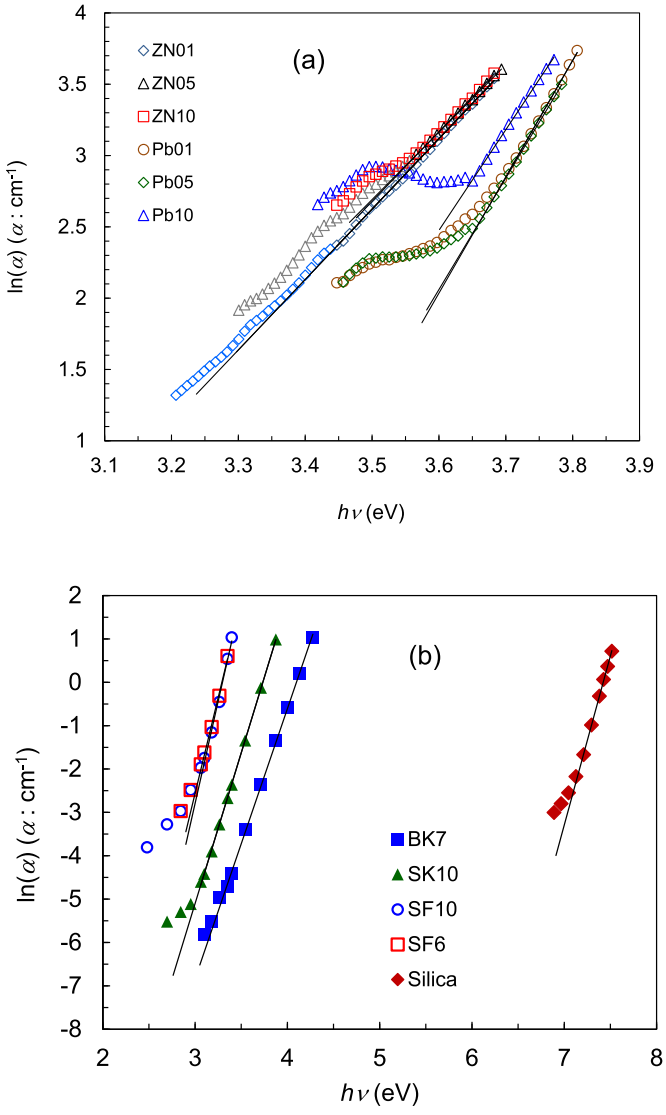

Fig. 5. Plots of lnα versus hν for (a) ZNbKLSNd and PbNKLSNd glasses and (b) other multi-component glasses. The slope of linearly fitted line gives the Urbach energy.

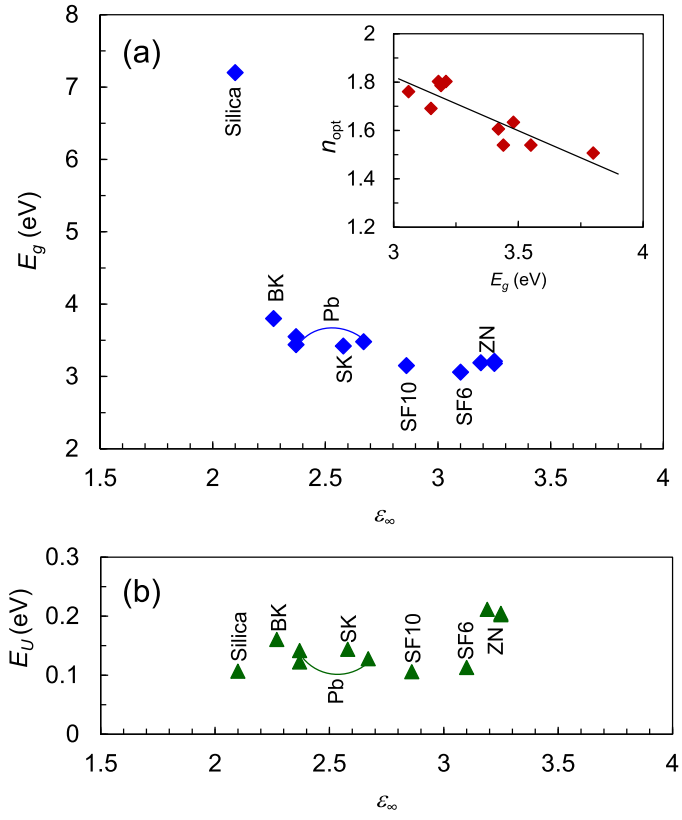

Fig. 6. Plots of (a) the optical bandgap energy E_g and (b) Urbach energy E_U as functions of the optical dielectric constant ε_∞. The inset of Fig. 6(a) shows the dependence of the optical refractive index n_{opt} on E_g for multi-component glasses other than silica, and the straight line indicates their linear fit.

3.3. Relationship between dielectric constant and energy gap

The relationship between the energy gap and dielectric constant can be studied by using the macroscopic energy gap picture proposed by Penn [16]. Penn gap model is based on an isotropic, nearly free electron model for the dielectric function which is characterized by an average energy difference between the conduction and valence bands called Penn gap. The dielectric constant at high frequency (optical frequency) ε_∞ is given by Penn [16] and PVV theory [15,32]:

$$\varepsilon_\infty = 1 + \left(\frac{\hbar\omega_p}{E_P}\right)^2 S_0, \quad (7)$$

where ω_p is the valence-electron plasmon frequency, E_P is the Penn gap and S_0 is a factor weakly dependent on the band gap. The valence-

electron plasmon energy, $\hbar\omega_p$ (eV), is given by [12,33]:

$$\hbar\omega_p = \hbar\left(\frac{NN_{eff}e^2}{\varepsilon_0 m}\right)^{1/2} = \hbar\left(\frac{N_A N_{eff}e^2}{V_m\varepsilon_0 m}\right)^{1/2} = 28.8\left(\frac{N_{eff}}{V_m}\right)^{1/2}, \quad (8)$$

where N_{eff} is the effective number of valence electrons per molecule, and V_m is the molar volume in cm^3/mol. N_{eff} is calculated by N_e=Ma+N(8-b) for a binary compound A_MB_N, where a(b) is the number of valence electrons per atom of type A(B) and M(N) is the atomic fraction of element A(B). According to Phillips' dielectric theory [33], the Penn gap is separated into the homopolar (E_h) and heteropolar (C) parts as is written as $E_P^2 = E_h^2 + C^2$. The ionic character of the bond is defined by the Phillips' ionicity parameter f_i by:

$$f_i = \frac{C^2}{E_h^2 + C^2}, \quad (9)$$

where E_h is related to the static dielectric constant ε_s, which is determined at the frequency sufficiently lower than all the oscillator resonance frequencies, by [34,35]:

$$\varepsilon_s = 1 + \left(\frac{\hbar\omega_p}{E_h}\right)^2 S_0. \quad (10)$$

We can determine the energies E_P, E_h and C and the ionicity parameter from ε_∞ and ε_s by using Eqs. (7)-(10). In this estimation, S_0 has been assumed to be a constant (0.6) according to [36,37]. The value of Z_{eff} is found to be 8 for SiO_2 and the same value has been used by assuming that the networks in all silicate oxide glasses examined here are governed by the same SiO_4-based network structure. The low frequency dielectric constant ε_s has been measured by using THz-TDS method as reported by us [7,8] and Naftaly et al. [5]. The values of ε_s and all the evaluated parameters are summarized in Table 3. To see the trend of variation, E_P, E_h and C as well as the measured value of E_g are shown in Fig. 7 as functions of the optical dielectric constant ε_∞. All four parameters decrease as ε_∞ increases. The homopolar energy E_h is found to approximately coincide with E_g over the whole range of ε_∞. This is considered to support that both of the optical and THz dielectric constants are consistently evaluated from the PVV model. On the other hand, since E_g (and E_h) exhibits a sharp drop as soon as additive components are introduced into pure silica, the heteropolar energy C becomes large and very close to the value of E_P, resulting in a very large Phillips ionicity parameter f_i for most of multi-component glasses as seen in Table 3. The value of f_i for silica (0.613) is consistent with the reported values [10,26], but as ε_∞ increases f_i becomes insensitive to the ε_∞ variation. Such high, saturating values of the ionicity parameter in those multi-component silicate oxide glasses are not consistent with our previous results obtained from THz-TDS analysis.

Here we return to the relationship between the optical dielectric constant and bandgap energy in the light of Eqs. (7) and (8). In Table 3, E_P is found to be proportional to E_h and the ratio $k = E_P/E_h$ is estimated to be 2.28 on average for all multi-component glasses (except silica). Knowing that $E_h \simeq E_g$ and considering that the glass dependence of V_m and therefore of $\hbar\omega_p$ is not very strong, $(\varepsilon_\infty - 1)^{1/2}$ is considered to be inversely proportional to E_g. According to this consideration, we show the plot of $1/(\varepsilon_\infty - 1)^{1/2}$ as a function of E_g (eV) in Fig. 8. A straight line can be fitted to the data as shown in Fig. 8 using the expression proposed by Herve and Vandamme [38]:

$$\varepsilon_\infty = 1 + \left(\frac{r_1}{E_g + r_2}\right)^2, \quad (11)$$

where r_1 and r_2 are constants. The values determined from Fig. 8 are $r_1 = 2.997$ and $r_2 = -1.071$. Although it is not appropriate to compare the fitting methods (Fig. 6, Fig. 8, etc.) within a narrow range of dielectric constant variation, the above result would be consistent with the physical background of the relation.

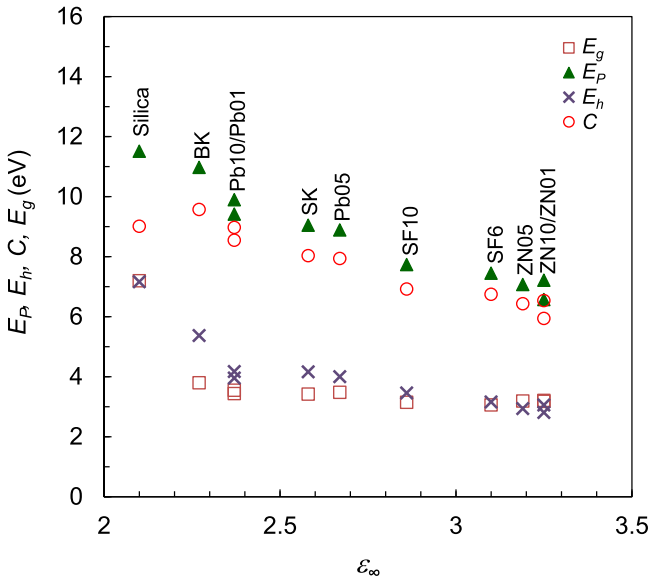

Fig. 7. Relationships of the Penn gap energy E_P, homopolar energy E_h, heteropolar energy C and the optical bandgap energy E_g as functions of the optical dielectric constant ε_∞ for different multi-component glasses.

3.4. Evaluation of ionicity effects

In order to look into the ionicity effect on the dielectric property, we investigate further the optical dielectric constant using the method developed by WDD [14]. The dispersion energy E_d in Eq. (1) indicates the strength of interband optical transition and has been found not to

Table 3
The THz dielectric constant (ε_s), valence electron plasmon energy ($\hbar\omega_p$), Penn gap energy (E_P), homopolar energy (E_h), heteropolar energy (C), Phillips ionicity parameter (f_i), Wemple DiDomenico ionicity parameter (β_1, β_2, β_3) and polarization ionicity measured from THz measurement (I_P).

Glass	ε_s	$\hbar\omega_p$ (eV)	E_P (eV)	E_h (eV)	E_P/E_h (*Av. k* = 2.28)	E_0/E_h (*Av.* k' =2.10)	C (eV)	f_i	β_1 (eV)	β_2 (eV)	β_3 (eV)	I_P
ZNbKLSNd01	13.54	14.00	7.22	3.06	2.36	2.02	6.54	0.821	0.261	0.272	0.313	0.465
ZNbKLSNd05	13.69	13.51	7.07	2.94	2.41	1.93	6.43	0.827	0.233	0.252	0.302	0.476
ZNbKLSNd10	13.32	12.73	6.57	2.81	2.34	2.21	5.94	0.817	0.263	0.250	0.310	0.468
PbNKLSNd01	8.70	14.96	9.90	4.17	2.37	1.45	8.98	0.822	0.157	0.226	0.211	0.544
PbNKLSNd05	9.24	14.84	8.89	4.00	2.22	1.54	7.94	0.797	0.194	0.264	0.252	0.515
PbNKLSNd10	8.76	14.23	9.42	3.96	2.38	1.84	8.55	0.823	0.189	0.214	0.204	0.572
silica	3.84	15.59	11.51	7.16	1.61	1.87	9.01	0.613	0.277	0.316	0.343	0.437
Pyrex	4.43	15.45		6.46								0.477
BK7	6.30	15.97	11.0	5.37	2.04	2.40	9.57	0.760	0.308	0.270	0.209	0.524
SK10	8.47	14.68	9.05	4.16	2.17	2.86	8.04	0.788	0.354	0.260	0.234	0.508
SF10	10.30	13.62	7.74	3.46	2.24	2.43	6.92	0.800	0.294	0.254	0.254	0.472
SF6	12.67	13.94	7.45	3.16	2.36	2.53	6.75	0.820	0.316	0.262	0.278	0.458

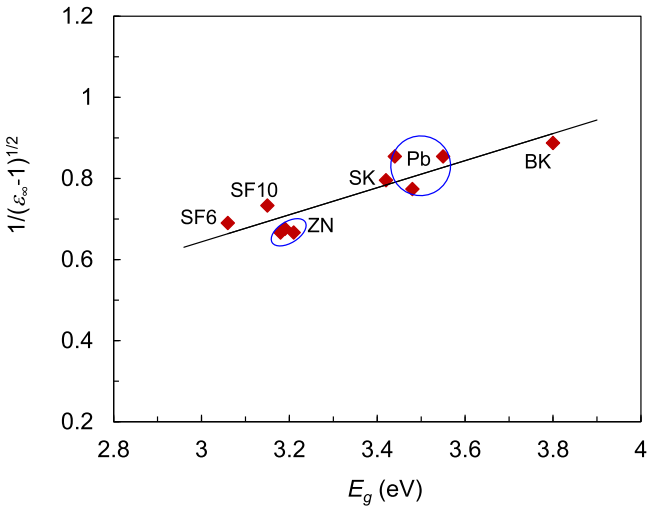

Fig. 8. Dependence of $1/(\varepsilon_\infty-1)^{1/2}$ on the bandgap energy E_g. The straight line fitted to the data indicates an approximation based on Herve and Vandamme model.

depend significantly on the bandgap energy and material structure or density [14], which is also confirmed from Table 2. It has been shown over a large number of crystalline materials [14] and also amorphous materials [39] that E_d is described by [40]:

$$E_d = \beta N_c Z_a N_{eff} \rho/\rho_c, \tag{12}$$

where N_c is the coordination number of the cations nearest to the anion, Z_a is the formal chemical valency of the anion, and N_{eff} is the effective number of valence electrons per molecule, ρ/ρ_c is the ratio of the density of vitreous material to the density of crystalline material, and β is a constant to represent the ionicity. The value of β has been found to exhibit $\beta_i = 0.26 \pm 0.04$ eV for ionic crystalline materials including halides and many oxides and $\beta_c = 0.37 \pm 0.05$ eV for crystalline materials with higher covalency [14]. In the Phillips' model Eq. (7) and ((8)), the dielectric constant is related with the material's physical structure through V_m. In contrast, E_d in WDD model is independent of both the physical structure and energy gap, and is more directly correlated with the material's chemical bond (N_c, Z_a) and ionicity (β). E_d can be correlated with the optical dielectric constant ε_∞ using Eq. (1) for $h\nu \to 0$ and this has been also confirmed already in Fig. 2. This follows the relation:

$$\varepsilon_\infty - 1 = \frac{E_d}{E_0} = \frac{\beta N_c Z_a N_{eff} \rho/\rho_c}{E_0}. \tag{13}$$

To determine β from Eq. (13), we use the parameter values of $N_c = 4$, $Z_a = 2$ and $N_{eff} = 8$ for silica glass [14] and the same also for all other multi-component silicate oxide glasses. This could be a rude assumption when the glass network based on the SiO_4 tetrahedral structure is modified too heavily by the introduction of multiple additive oxides. However, as WDD has reported in [39], in several silicate glasses containing different additives (e.g., Na_2O, K_2O, PbO, BaO, CaO; the fraction of SiO_2 >50% mol), E_d value is fairly independent of the composition and additive species, and therefore the same $N_c Z_a N_{eff}$ value is considered to be maintained in Pyrex, BK, SK and SF glasses as well. As for OFS glasses studied here, the fraction of SiO_2 is more than 30% mol and the E_d values evaluated are not far from those of other oxide glasses. In addition, a strong increase of E_d (e.g. >20 eV) as reported by WDD [14, 39] for oxide crystals containing high-coordination number cations [14] and rare earth cations (e.g. La [39]) has not been found in our study. Taking those observations into account, it would be allowed to apply the value of $N_c Z_a N_{eff}$ same as that for Si for all multi-component glasses examined here. For the density ratio ρ/ρ_c, we consider the quartz ($\rho_c = 2.65$ g/cm^3 [11,39,40]) and fused silica ($\rho = 2.20$ g/cm^3 [5,39,40]), and use this ratio ($\rho/\rho_c = 0.83$) for all multi-component glasses.

For deriving β from Eq. (13), we have examined three ways of estimating E_0. Firstly one can directly use the value of E_0 as evaluated from the optical dispersion for determining β (β_1). In the second approach (β_2), the value of E_h as determined from the THz dielectric constant is used. Considering that both E_0 and E_P are basically interpreted as the energy of dominant imaginary part of the optical dielectric constant, E_0 is assumed to be replaceable with E_P. Using a good approximation of $E_P = kE_h$ ($k = 2.28$) as described in the previous section, E_0 can therefore be estimated by $E_0 = k'E_h$. The average value of $k' = E_0/E_h$ is given to be 2.10 (+0.76, −0.65) as shown in Table 3. In the third approach (β_3), the optical bandgap energy E_g is used. By further applying the approximation of $E_h \simeq E_g$, E_0 can be evaluated by $E_0 = k''E_g$. The average value of $k'' = E_0/E_g$ is given to be 2.28 (+0.67, −0.08) as shown in Table 2.

For illustrating the procedure of the third approach, the plot of $\varepsilon_\infty - 1$ as a function of $1/E_g$ is shown in Fig. 9. The slope made by each data point and the origin, or the value of $(\varepsilon_\infty - 1)E_g$, determines the value of β (β_3) for each glass. Two straight lines in the figure correspond to the covalent ($\beta_c = 0.37$) and ionic ($\beta_i = 0.26$) lines, respectively. Silica indicates a β value close to the covalent value, and most of other glasses show β values closer to the ionic value. The estimated results of β using three approaches (β_1, β_2 and β_3) are shown in Table 3. The relation $E_0 = k''E_g$ as used in the third approach has been verified in many works in literature, though somewhat different k" values have been reported for different materials. For example, $k'' = 1.5$ has been found for numbers of crystalline solids [14], 1.7 for SiO_xN_y non-crystalline films [41], 1.9 for chalcogenide glasses [42], 1.8–2.3 for TiO_2 amorphous films [43,44], and 2.2–2.5 for iridium oxide polycrystalline films [45].

In our most recent study [9], we have demonstrated the essential role of the polarization ionicity I_P in characterizing the THz dielectric constant in glass materials. I_P is defined as the ionic (or lattice vibration induced) contribution fraction in the total microscopic susceptibility (which consists of the electronic and ionic contributions) and is determined straightforwardly from the optical (ε_∞) and THz dielectric constant (ε_s) values by a simple relation [9]:

$$I_p = \frac{3(\varepsilon_s - \varepsilon_\infty)}{(\varepsilon_s - 1)(\varepsilon_\infty + 2)}. \tag{14}$$

In Fig. 10, all the values of β determined by three approaches are plotted as functions of I_P. A straight line in the figure shows a linear fit of β (β_1)

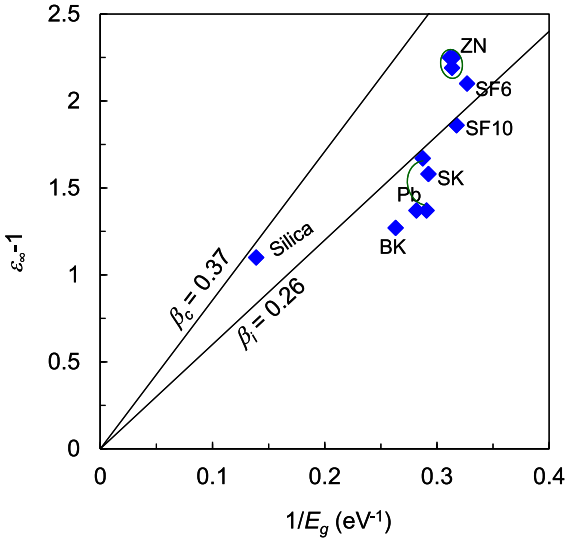

Fig. 9. Relation of $\varepsilon_\infty - 1$ as a function of $1/E_g$ for different glasses. The slope made by the origin and each data point is proportional to the Wemple and DiDomenico parameter for ionicity, β. Two lines show representative slopes for ionic (β_i) and covalent (β_c) characteristics.

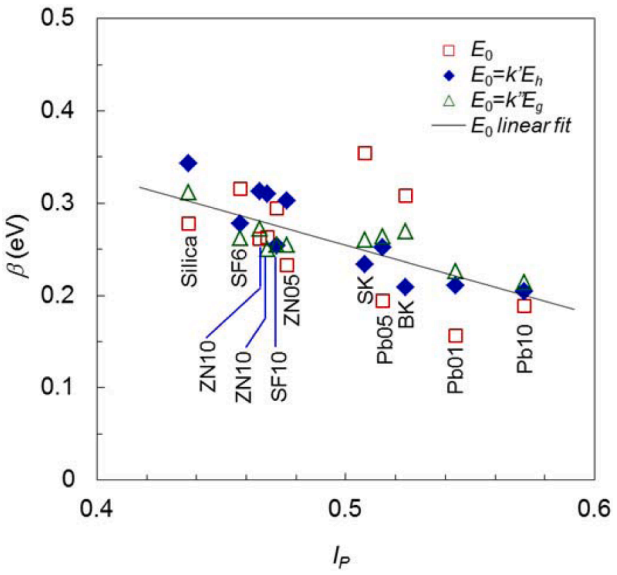

Fig. 10. Relationships of the values of ionicity parameter β determined by three approaches as functions of the polarization ionicity I_P determined from THz measurement. A straight line in the figure shows a linear fit of β (β_1) obtained from the $\varepsilon_\infty - 1$ versus $1/E_0$ relationship.

obtained from E_0. The most important message of Fig. 10 is in that, although β_1 exhibits appreciable scattering, all β values evaluated by three different approaches based on optical and THz measurements indicate a consistent interrelation with I_P regardless of the large difference of glass compositions. It is interesting to note that β and I_P do not show a saturating behavior which is noticed for the Phillips' ionicity f_i in the large f_i region (as is observed in Table 3). The monotonous dependence of β on I_P as observed here suggests that β can be used as an indicator for the strength of ionicity rather than a discrete-valued parameter. In particular, the use of Eq. (13) together with $E_0 = k''E_g$ (the third approach) enables the determination of β using only the optical dielectric and energy properties as far as the chemical bond parameters ($N_c Z_a N_{eff}$) can be assumed.

In contrast with the present results, previous attempts to correlate the ionicity with a certain single parameter such as the Pauling's bond ionicity parameter (I_b as defined by the cation-anion electronegativity difference) [10] or the optical electronegativity (as defined through the optical refractive index) [46] face considerable limitations in applicability [39,40]. For example, no monotonous correlation has been found between I_P and I_b [9] on the same set of multi-component glasses as adopted in this work. Also, in the case of ionicity evaluation using the optical electronegativity (defined by the optical refractive index), different equations had to be used for characterizing different groups of material structures (e.g., silica vs. other SiO_2 polymorphs) [46]. In contrast to those parameters, the present β parameter, which primarily reflects the dielectric dispersion nature of the material, is reasonably understood to be capable of covering wider variety of materials.

3.5. Joint density of states in glasses

We have seen so far a strong interlink between the optical dielectric constant and the bandgap energy, which implies the critical effects of the band structure. In order to have an insight about the band structure, we discuss in the following the joint density of states (JDOS) which is defined by the convolution of DOS for two bands:

$$JDOS(E) = \int N_v(E')N_c(E'+E)dE', \quad (15)$$

where $N_v(E')$ and $N_c(E)$ are the valence band DOS and conduction band DOS at the energy E' and E, respectively. JDOS(E) is estimated by considering all the energy parameters obtained in the present study, and the schematic illustration of JDOS(E) are shown for four representative glasses in Fig. 11. E_P represents a macroscopic gap accounting for all the possible optically induced electronic transitions in the material. E_0 is an average energy to excite electrons from the valence band to conduction band coinciding with the energy for the maximum of the imaginary part of dielectric constant ε_2 in the ε_2 –E spectra. E_P and E_0 are both in the vicinity of the ε_2 peak, but their exact values could fluctuate. For example, a few investigators reported that E_P agrees reasonably well with the average energy of a few peaks appearing in the broadband reflectance spectra (indicating transitions) [35,47,48]. In our result, an alteration in the relation between E_P and E_0 is noticed among four glasses; $E_P > E_0$ for silica and SK glass, and $E_P < E_0$ for other glasses. This is presumed to be caused by the variation in the ε_2 spectral profile or in the DOS profiles within the two bands. At the energy near the onset of ε_2 or JDOS, an abrupt change occurs in the absorption spectra. E_g which is determined from the Tauc plot represents the energy of the onset of JDOS increase indicating the electronic transition between the valence band maximum and conduction band minimum, corresponding to the mobility gap. This absorption change is associated with the Urbach tail which indicates the existence of localized states in the forbidden gap. Those sub-gap states are spatially isolated and may not directly contribute to the conduction but can contribute to optical transition. We have seen that E_g and E_h exhibit very close values. Taking into account that E_h is determined from the valence-electron plasmon energy (Eq. (10)) rather than from the optical transition spectra, E_h is tentatively interpreted to correspond to the energy at the abrupt JDOS onset: E_g.

In oxide materials, the valence band consists of oxygen anion's 2p orbitals with strong spatial directivity. When structural or compositional disorders are introduced in the oxides, bonds are physically or chemically strained, leading to the generation of localized states above the valence band maximum. In contrast, the conduction band is made of metal cation's s orbitals with spherically symmetric envelope, and the overlap of s orbitals between neighboring metal atoms is not influenced significantly by structural fluctuations (neglecting the d orbital electron effects). Therefore the electronic states below the conduction band minimum are insensitive to disorders [49]. Thus the sub-gap localized states as revealed by the Urbach tails in the present glasses are considered to be primarily associated with the valence band. It has also been reported that most of the defects found in silica and silicate oxide materials are oxygen related; i.e., oxygen deficiency induced cation (Si) dangling bonds or excess oxygen induced non-bridging oxygens [50,51]. Several different localized states have been found to form above the valence band [51]. E_U values determined in the present glasses coincide with the ones already reported for silica glasses (0.06–0.18 eV [52,53]). The Urbach tails observed here are thus presumed to originate from such anion structural disorder induced localized states.

Among all of the present glasses, ZNbKLSNd glasses have shown E_U

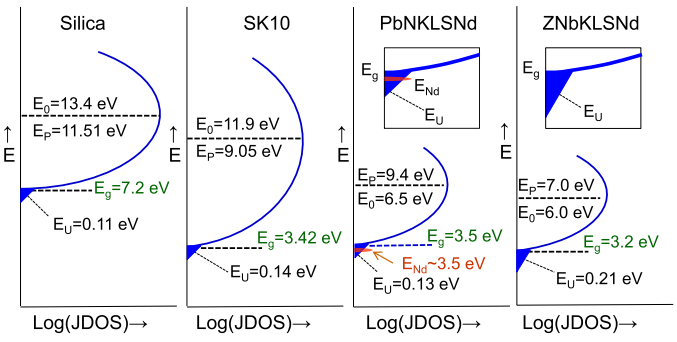

Fig. 11. Schematic illustration of the joint density of states JDOS(E) versus energy for four representative glass materials. Insets show close-up views near the bandgap energies for PbNKLSNd and ZNbKLSNd glasses.

(0.21 eV) considerably higher than others. The largest V_m, lowest E_g and highest ε_{opt} of ZNbKLSNd glasses may be consistent with the introduction of higher degree of structural disorders. ZNbKLSNd glasses have a low ionicity (I_P = 0.465–0.476) as low as that of silica (I_P = 0.437), meaning their fairly strong covalent nature. In covalent materials, e.g. amorphous Si:H, the conduction and valence bands comprise of Si sp^3 orbitals with high spatial directivity. Therefore, when their chemical bands are strained, high density localized states can be generated [49,54]. The fairly high covalent nature of ZNbKLSNd glasses would be responsible for the higher Urbach energy.

PbNKLSNd glasses are unique in that they exhibit appreciably strong shoulders in absorption spectra at ~3.5 eV (Fig. 4(b) and Fig. 5(a)). The shoulder observed is considered not due to the interband transition absorption but attributable to the atomic multiplet absorption of Nd atom ($^4D_{1/2}$ + $^4D_{3/2}$ + $^4D_{5/2}$) [55,56]. This interpretation is consistent with that the absorption peak intensity increases in parallel with the Nd_2O_3 composition (x) increase, and also that absorption shoulders are recognized at the same photon energy also in ZNbKLSNd glasses which incorporate Nd_2O_3 (Fig. 4(a) and Fig. 5(a)). In PbNKLSNd and SK10 glasses, the Urbach energy is comparatively restrained. This is likely caused by the high ionicity (I_P = 0.508–0.572) of these glasses, which exhibits an apparent contrast to ZNbKLSNd glasses.

4. Conclusions

In order to obtain comprehensive understanding of the physical properties of a variety of multi-component silicate oxide glasses containing vastly different additive components, both the optical- and THz-spectroscopic characterizations have been utilized. The dielectric constant and energy band parameters have been determined from the optical data on the basis of the single oscillator based WDD model. Using those results, a common tradeoff relationship has been found between the oscillator strength and characteristic resonant wavelength. It has been shown that the optical bandgap energy (E_g) coincides with the homopolar energy (E_h) deduced from PVV dielectric model by using the THz dielectric constant. Also an expression has been determined to correlate the optical dielectric constant (ε_∞) with the bandgap energy (E_g) for all multi-component glasses (except pure silica). The ionicity parameters evaluated from the optical (β) and THz (I_P) measurements have been compared and a reasonable correspondence has been confirmed. Thus a comprehensive interrelation has been confirmed among the determined physical parameters over a wide range of multi-component silicate oxide glasses regardless of the vast difference in additive species. The energy band parameters estimated have been applied to obtain the joint density of state diagrams for representative glasses, and physical/chemical natures specific to respective glasses have been identified.

CRediT authorship contribution statement

Osamu Wada: Conceptualization, Formal analysis, Investigation, Writing – original draft, Writing – review & editing. **Doddoji Ramachari:** Methodology, Data curation, Formal analysis, Writing – review & editing. **Chan-Shan Yang:** Methodology, Data curation, Writing – review & editing. **Ci-Ling Pan:** Funding acquisition, Resources, Supervision, Writing – review & editing.

Declaration of Competing Interest

The authors declare that they have no known competing financial interests or personal relationships that could have appeared to influence the work reported in this paper.

Acknowledgments

The authors are thankful to Ministry of Science and Technology, Taiwan for funding support to the present research (# MOST 106–2112-M-007–022-MY2, # MOST 110–2923-E-007–006). Doddoji Ramachari is thankful to Ministry of Science and Technology, Taiwan for the award of Postdoctoral Fellowship during this research work. The authors thank Chao-Kai Wang and Chun-Ling Yen for taking the THz-TDS data of the samples reported in this work. Osamu Wada thanks to Japan Society for the Promotion of Science (JSPS KAKENHI Grant Number JP19K04532) for supporting this publication.

References

[1] M. Zalkovskij, A.C. Strikwerda, K. Iwaszczuk, A. Popescu, D. Savastru, R. Malureanu, A.V. Lavrinenko, P.U. Jepsen, Terahertz-induced Kerr effect in amorphous chalcogenide glasses, Appl. Phys. Lett. 103 (22) (2013), 221102, https://doi.org/10.1063/1.4832825.

[2] M.S. Islam, C.M.B. Cordeiro, M.J. Nine, J. Sultana, A.L.S. Cruz, A. Dinovitser, B.W.-H. Ng, H. Ebendorff-Heidepriem, D. Losic, D. Abbott, Experimental study on glass and polymers: determining the optimal material for potential use in terahertz technology, IEEE Access 8 (2020) 97204–97214, https://doi.org/10.1109/ACCESS.2020.2996278.

[3] B. You, J.-Y. Lu, C.-P. Yu, T.-A. Liu, J.-L. Peng, Terahertz refractive index sensors using dielectric pipe waveguides, Opt. Express 20 (6) (2012) 5858–5866, https://doi.org/10.1364/OE.20.005858.

[4] S. Singla, V.G. Achanta, N. Mahendru, S.S. Prabhu, M. Falconieri, G. Sharma, High refractive index gold nanoparticle doped Bi_2O_3-B_2O_3 glasses for THz frequencies", Opt. Mater. (Amst.) 72 (2017) 91–97, https://doi.org/10.1016/j.optmat.2017.05.043.

[5] M. Naftaly, R.E. Miles, Terahertz time-domain spectroscopy of silicate glasses and the relationship to material properties, J. Appl. Phys. 102 (4) (2007) 1–6, https://doi.org/10.1063/1.2771049, 043517.

[6] A. Ravagli, M. Naftaly, C. Craig, E. Weatherby, D.W. Hewak, Dielectric and structural characterisation of chalcogenide glasses via terahertz time-domain spectroscopy, Opt. Mater. (Amst.) 69 (2017) 339–343, https://doi.org/10.1016/j.optmat.2017.04.057.

[7] D. Ramachari, C.-.S. Yang, O. Wada, T. Uchino, C.-.L. Pan, High-refractive index, low-loss oxyfluorosilicate glasses for sub-THz and millimeter wave applications, J. Appl. Phys. 125 (15) (2019) 1–8, https://doi.org/10.1063/1.5083091, 151609.

[8] O. Wada, D. Ramachari, C.-.S. Yang, T. Uchino, C.-.L. Pan, High refractive index properties of oxyfluorosilicate glasses and a unified dielectric model of silicate oxide glasses in sub-Terahertz frequency region, Opt. Mater. Express 10 (2) (2020) 607–621, https://doi.org/10.1364/OME.382686.

[9] O. Wada, D. Ramachari, C.-.S. Yang, T. Uchino, C.-.L. Pan, Systematic characterization of THz dielectric properties of multi-component glasses using unified oscillator model, Opt. Mater. Express 11 (3) (2021) 858–874, https://doi.org/10.1364/OME.417771.

[10] J.A. Duffy, Chemical Bonding in the Oxides of the Elements: a New Appraisal, J. Solid State Chem. 62 (2) (1986) 145–157, https://doi.org/10.1016/0022-4596(86)90225-2.

[11] V. Dimitrov, Electronic oxide polarizability and optical basicity of simple oxides. I, J. Appl. Phys. 79 (3) (1996) 1736–1740, https://doi.org/10.1063/1.360962.

[12] N.M. Ravindra, Energy gap-refractive index relation—Some observations", Infrared Phys. 21 (1981) 283–285, https://doi.org/10.1016/0020-0891(81)90033-6.

[13] J. McCloy, B. Riley, B. Johnson, M. Schweiger, H.A. Qiao, The Predictive Power of Electronic Polarizability for Tailoring the Refractivity of High-Index Glasses: optical Basicity Versus the Single Oscillator Model, J. Am. Ceramic Soc. 93 (6) (2010) 1650–1662, https://doi.org/10.1111/j.1551-2916.2010.03613.x.

[14] S.H. Wemple, M. DiDomenico, Behavior of the Electronic Dielectric Constant in Covalent and Ionic Materials, Phys. Rev. B 3 (4) (1971) 1338–1351, https://doi.org/10.1103/PhysRevB.3.1338.

[15] J.C. Phillips, J.A. Van Vechten, Dielectric Classification of Crystal Structures, Ionization Potentials, and Band Structures, Phys. Rev. Lett. 22 (1969) 705, https://doi.org/10.1103/PhysRevLett.22.705.

[16] D.R. Penn, Wave-Number-Dependent Dielectric Function of Semiconductors, Phys. Rev. 128 (5) (1970) 2093, https://doi.org/10.1103/PhysRev.128.2093.

[17] C.-S. Yang, M.-H. Lin, C.-H. Chang, P. Yu, J.-M. Shieh, C.-H. Shen, O. Wada, C.-L. Pan, Non-Drude Behavior in Indium-Tin-Oxide Nanowhiskers and Thin Films Investigated by Transmission and Reflection THz Time-Domain Spectroscopy, IEEE J. Quantum Electron. 49 (8) (2013) 677–690, https://doi.org/10.1109/JQE.2013.2270552.

[18] Schott, Optical Glass Data Sheets: https://www.schott.com/d/advanced_optics/ac85c64c-60a0-4113-a9df-23ee1be20428/1.17/schott-optical-glass-collection-datasheets-english-may-2019.pdf, and https://www.schott.com/d/advanced_optics/555cd92f-3839-4605-b12c-be3cf34c4e03/1.8/schott-optical-glass-inquiry-glass-collection-datasheets-english-03032017.pdf (accessed 10.8. 2021).

[19] Refractiveindex. info database: refractiveIndex.INFO - Refractive index database https://refractiveindex.info/(accessed 10.8. 2021).

[20] Optical Characteristics (ES), Silica Glass, Tosoh Quartz Corporation, 2021. http://www.tqgj.co.jp/en/silicaglass/ (accessed 10.8.2021).

[21] G.B. Sakr, I.S. Yahia, M. Fadel, S.S. Fouad, N. Romcevic, Optical spectroscopy, optical conductivity, dielectric properties and new methods for determining the gap states of CuSe thin films, J. Alloys Compd. 507 (2010) 557–562, https://doi.org/10.1016/j.jallcom.2010.08.022.

[22] H. Takebe, S. Fujino, K. Morinaga, Refractive-Index Dispersion of Tellurite Glasses in the Region from 0.40 to 1.71 μm", J. Am. Ceram. Soc. 77 (9) (1994) 2455–2457, https://doi.org/10.1111/j.1151-2916.1994.tb04621.x.
[23] S. Hirota, T. Izumitani, Effect of cations on the inherent absorption wavelength and the oscillator strength of ultraviolet absorptions in borate glasses, J. Non Cryst. Solids 29 (1) (1978) 109–117, https://doi.org/10.1016/0022-3093(78)90144-8.
[24] S. Fujino, H. Takebe, K. Morinaga, Measurements of refractive indexes and factors affecting dispersion in oxide glasses, J. Am. Ceramic Soc. 78 (5) (1995) 1179–1184, https://doi.org/10.1111/j.1151-2916.1995.tb08466.x.
[25] J. Tauc, Chap.4 Optical properties of amorphous semiconductors, in: J. Tauc (Ed.), Amorphous and Liquid Semiconductors, Plenum Press, London and New York, 1974, https://doi.org/10.1007/978-1-4615-8705-7.
[26] K. Saito, A.J. Ikushima, Absorption edge in silica glass, Phys. Rev. B 62 (13) (2000) 8584–8587, https://doi.org/10.1103/PhysRevB.62.8584.
[27] F.J. Ferrer, F. Yubero, J.A. Mejías, F.J. García-Lopez, A.R. González-Elipe, Microscopic and macroscopic dielectric description of mixed oxide thin films, J. Appl. Phys. 102 (2007), 084112, https://doi.org/10.1063/1.2801402.
[28] K. Terashima, T. Hashimoto, T. Uchino, S. -H.Kim, T. Yoko, Structure and Nonlinear Optical Properties of Sb2O3-B2O3 Binary Glasses, J. Ceram. Soc. Japan 104 (11) (1996) 1008–1014, https://doi.org/10.2109/jcersj.104.1008.
[29] I. Jlassi, H. Elhouichet, M. Ferid, Thermal and optical properties of tellurite glasses doped erbium, J. Mater. Sci. 46 (2011) 806–812, https://doi.org/10.1007/s10853-010-4820-x.
[30] N.M. Ravindra, R.P. Bhardwaj, K. SunilKumar, V.K. Srivastava, Model based studies of some optical and electronic properties of narrow and wide gap materials, Infrared Phys. 21 (6) (1981) 369–381, https://doi.org/10.1016/0020-0891(81)90045-2.
[31] R. Ravichandran, A.X. Wang, J. F.Wager, Solid state dielectric screening versus band gap trends and implications, Opt. Mater. (Amst) 60 (2016) 181–187, https://doi.org/10.1016/j.optmat.2016.07.027.
[32] J.C. Phillips, Ionicity of the Chemical Bond in Crystals, Rev. Mod. Phys. 42 (3) (1970) 317, https://doi.org/10.1103/RevModPhys.42.317.
[33] J.D. Jackson, Classical Electrodynamics, 3rd Ed, John Wiley & Sons, Inc., New York, 1998, p. 313. ISBN 978-0-471-30932-X.
[34] J.C. Phillips, Bonds and Bands in Semiconductors, Academic Press, New York, 1973, p. 35, https://doi.org/10.1016/B978-0-12-553350-8.X5001-5. ISBN: 978-0-12-553350-8.
[35] C. Lamsal, N.M. Ravindra, Optical properties of vanadium oxides-an analysis, J. Mater. Sci. 48 (2013) 6341–6351, https://doi.org/10.1007/s10853-013-7433-3.
[36] R.D. Grimes, E.R. Cowley, A model dielectric function for semiconductors, Can. J. Phys. 53 (23) (1975) 2549–2554, https://doi.org/10.1139/p75-311.
[37] R.R. Reddy, K.R. Gopal, K. Narasimhulu, L.S.S. Reddy, K.R. Kumar, C.V.K. Reddy, S.N. Ahmed, Correlation between optical electronegativity and refractive index of ternary chalcopyrites, semiconductors, insulators, oxides and alkali halides, Opt Mater (Amst) 31 (2) (2008) 209–212, https://doi.org/10.1016/j.optmat.2008.03.010.
[38] P. Hervé, L.K.J. Vandamme, General relation between refractive index and energy gap in semiconductors, Infrared Phys. Technol. 35 (4) (1994) 609–615, https://doi.org/10.1016/1350-4495(94)90026-4.
[39] S.H. Wemple, Refractive-index behavior of amorphous semiconductors and glasses, Phys. Rev. B 7 (8) (1973) 3767–3777, https://doi.org/10.1103/PhysRevB.7.3767.
[40] S.H. Wemple, D.A. Pinnow, T.C. Rich, R.E. Jaeger, L.G. Van Uitert, Binary SiO_2–B_2O_3 glass system: refractive index behavior and energy gap considerations, J. Appl. Phys. 44 (1973) 5432–5437, https://doi.org/10.1063/1.1662170.
[41] M. Modreanu, M. Gartner, N. Tomozeiu, A. Szekeres, "Optical and Electrical Properties of As-Deposited LPCVD SiOxNy Thin Films", J. Optoelectron. Adv. Mater. 3(2), 575–580 (2001).
[42] K. Tanaka, Optical properties and photoinduced changes in amorphous As-S films, Thin Solid Films 66 (3) (1980) 271–279, https://doi.org/10.1016/0040-6090(80)90381-8.
[43] W. Naffouti, T.B. Nasr, O. Briot, N. Kamoun-Turki, Effect of sprayed solution volume on physical properties of titanium dioxide thin films, J. Electron. Mater. 44 (10) (2015) 3661–3669, https://doi.org/10.1007/s11664-015-3878-2.
[44] A.S. Hassanien, A.A. Akl, Optical characterizations and refractive index dispersion parameters of annealed TiO_2 thin films synthesized by RF-sputtering technique at different flow rates of the reactive oxygen gas", Physica B 576 (2020) https://doi.org/10.1016/j.physb.2019.411718, 411718/1-13.
[45] O. Gençyılmaz, F. Atay, I. Akyuz, Production and characterization of iridium oxide films by ultrasonic chemical spray pyrolysis, J. Optoelectron. Adv. Mater. 17 (3–4) (2015) 395–402.
[46] R.R. Reddy, K.R. Gopala, Y.N. Ahammed, K. Narasimhulu, L.S.S. Reddy, C.V. K. Reddy, Correlation between optical electronegativity, molar refraction, ionicity and density of binary oxides, silicates and minerals, Solid State Ion. 176 (2005) 401–407, https://doi.org/10.1016/j.ssi.2004.07.041.
[47] N.M. Ravindra, J. Narayan, Optical properties of silicon related insulators, J. Appl. Phys. 61 (5) (1987) 2017–2021, https://doi.org/10.1063/1.337998.
[48] P. Singh, N.M. Ravindra, Optical properties of metal phthalocyanines, J. Mater. Sci. 45 (2010) 4013–4020, https://doi.org/10.1007/s10853-010-4476-6.
[49] Toshio Kamiya, Kenji Nomura, Hideo Hosono, Origins of high mobility and low operation voltage of amorphous oxide, J. Display Technol. 5 (7) (2009) 273–288, https://doi.org/10.1109/JDT.2009.2034559.
[50] F. Funabiki, T. Kamiya, H. Hosono, Doping effects in amorphous oxides, J. Ceram. Soc. Japan 120 (11) (2012) 447–457, https://doi.org/10.2109/jcersj2.120.447.
[51] K.T. Vogt, C.E. Malmberg, J.C. Buchanan, G.W. Mattson, G.M. Brandt, D.B. Fast, P. H.-Y. Cheong, J.F. Wager, M.W. Graham, Ultrabroadband density of states of amorphous In-Ga-Zn-O, Phys. Rev. Res. 2 (2020), https://doi.org/10.1103/PhysRevResearch.2.033358, 033358/1-11.
[52] R. Boscaino, E. Vella, G. Navarra, Absorption edge in silica glass, in: Proceedings of 2005 IEEE/LEOS Workshop on Fibres and Optical Passive Components, Palermo, Italy, 2005, https://doi.org/10.1109/WFOPC.2005.1462147. July.
[53] L. Skuja, K. Kajihara, Y. Ikuta, M. Hirano, H. Hosono, Urbach absorption edge of silica: reduction of glassy disorder by fluorine doping, J. Non Cryst. Solids 345–346 (2004) 328–331, https://doi.org/10.1016/j.jnoncrysol.2004.08.038.
[54] I. Umezu, K. Miyamoto, N. Sakamoto, K. Maeda, Optical Bond Gap and Tauc Gap in a-SiOx:H and a-SiNx:H Films, Jpn. J. Appl. Phys. 34 (4R) (1995) 1753–1758, https://doi.org/10.1143/JJAP.34.1753.
[55] P. Chimalawonga, J. Kaewkhaob, C. Kedkaewa, P. Limsuwanac, Optical and electronic polarizability investigation of Nd3+-doped soda-lime silicate glasses, J. Phys. Chem. Solids 71 (7) (2010) 965–970, https://doi.org/10.1016/j.jpcs.2010.03.044.
[56] M. Das Mukherjee, A. Kalyandurg, P. Kundu, R.N. Dwivedi, S. Buddhudu, Optical spectra of Nd3+:CaO–La2O3–B2O3 glasses", Mater. Lett. 60 (2) (2006) 222–229, https://doi.org/10.1016/j.matlet.2005.08.022.